A comparison of pulse and CW EPR T_2-relaxation measurements of an inhomogeneously broadened nitroxide spin probe undergoing Heisenberg spin exchange

Barney L. Bales*[1], Miroslav Peric[1], Daniel Kinzek[1], Robert N. Schwartz[2]

[1] Department of Physics and Astronomy, California State University at Northridge, Northridge, CA, 91330, USA. [2]Electrical and Computer Engineering Department, University of California, Los Angeles, Los Angeles, CA90095, USA.

Keywords: Heisenberg spin exchange, spin relaxation, nitroxide spin probes, pulse versus CW EPR.

ABSTRACT
Nitroxide spin probes are inhomogeneously broadened (IHB) by intramolecular hyperfine interactions with protons (deuterons) producing lines of Voigt shape. Thus, to study T_2 relaxation by continuous wave (CW) EPR, the Voigt must be deconvoluted to find the Lorentzian component. For homogeneously broadened lines, T_2 is obtained directly from the Lorentzian line widths ΔH_{pp}^{L}; however, for IHB lines finding T_2 from ΔH_{pp}^{L} is more complicated. It has been known for many years that values of ΔH_{pp}^{L} of high precision may be obtained from IHB lines; however, direct, accurate comparison of spin exchange frequencies obtained from electron spin echo decay and CW EPR data has been lacking. It is demonstrated here that despite complications in the interpretation of experiments, these two techniques yield the same spin exchange rate constant for spin probes that are the most difficult to treat.

1. Introduction

The study of spin relaxation of free radicals, T_1 and T_2, in solutions of relatively low viscosities continues to be an active field of study [1]. The recent book by Marsh [1] provides a wealth of experimental and theoretical information related to spin relaxation in nitroxide radicals. In recent years, most of the work has been performed using various pulsed-EPR techniques. In principle, the Hahn two-pulse primary spin-echo decay (ESE) technique can yield T_2 directly from the decay of the echo amplitude with pulse spacing [2]. In contrast, careful line shape analysis is required to extract T_2 in the CW EPR experiment [3, 4]. Some studies are designed to test theories [5-13] which are still being extended to interesting [14, 15] and "peculiar" [16-19] behaviors while others have practical goals in mind. An example of the latter is to seek a deeper understanding of the role of Heisenberg spin exchange (HSE) in Overhauser dynamic nuclear polarization (DNP) experiments [5, 13]. Here, we limit ourselves to nitroxide free radicals (nitroxides) executing rapid rotational and translation motion yielding spectra in the motionally narrowed regime. A renewed interest in CW EPR studies of spin relaxation is due to discoveries of interesting spectral properties of nitroxides where HSE introduces admixtures of absorptive (ABS) and dispersive (DIS) components: see e.g., refs [14, 20] and references therein. To study spin relaxation in the presence of these features, continuous wave saturation (CWS) methods have been shown to be applicable [15] while it is not clear how pulsed methods could be employed. It is particularly interesting to study the relaxation of DIS which has been measured and discussed only once [15].

An important first step is to ensure that the same value of the rate constant of HSE, K_{ex}, is obtained from CW EPR and ESE over a range of HSE that is accessible to both methods. For ESE [2], K_{ex} is obtained directly from the measured phase memory time T_M, which in the motionally narrowed regime is equal to the spin packet width T_2 [1, 2, 21].

All nitroxides, except Fremy's salt, are inhomogeneously broadened (IHB) by hyperfine interactions with protons (deuterons) and other magnetic nuclei [3]. Fortunately, these hyperfine structures are accurately modeled with a Gaussian (G) shape which when convoluted with the Lorentzian (L) shape yields the well-known Voigt (V) shape [3].

The purpose of this Communication is to compare quantitatively the results of K_{ex} obtained from CW EPR with those measured by ESE. To make the comparison for the most difficult lines to analyze, we have chosen 4-Hydroxy-2,2,6,6-tetramethylpiperidine-1-oxyl (H-Tempol) which has the largest IHB of the nitroxides commonly used [3]. Fortunately, ESE measurements are available in the literature [13] for H-Tempol in toluene, so we chose toluene as the solvent.

2. Theory

The relaxation time of the transverse magnetization in the presence of HSE, T_2^{eff}, is related to the Lorentzian line width of the CW spectrum by [21]

$$T_2^{eff} = 2/[\gamma\sqrt{3}\Delta H_{pp}^L(0)] \tag{1}$$

where $\Delta H_{pp}^L(0) = \lim_{H_1 \to 0} \Delta H_{pp}^L$ and γ the gyromagnetic ratio of the electron. T_2^{eff} may be obtained from ESE and $\Delta H_{pp}^L(0)$ from CW EPR; thus, the two may be compared for the same experimental conditions. All linewidths are peak-to-peak values of first-derivative spectra. To measure $\Delta H_{pp}^L(0)$ with improved precision [21], continuous wave saturation curves (CWS) may be measured and fit to the Bloch equations as follows:

$$\Delta H_{pp}^L = \Delta H_{pp}^L(0)\left(1 + H_1^2 \frac{2}{\sqrt{3}\Delta H_{pp}^L(0)} \gamma T_1^{eff}\right)^{1/2} \tag{2}$$

where H_1 is the circularly-polarized magnetic induction of the microwave field and Eq. 1 has been employed to replace the usual factor γT_2^{eff}. H_1 is proportional to $\sqrt{P}$, where P is the microwave power incident on the cavity. The constant of proportionality is determined by the procedure in ref [21].

For Fremy's salt, T_2^{eff} may be determined directly from the measured line widths because the lines are nearly L but for all other nitroxides the lines are IHB; thus, they are V shape which is defined uniquely by the Voigt parameter [3],

$$\chi = \frac{\Delta H_{pp}^G}{\Delta H_{pp}^L}. \tag{3}$$

ΔH_{pp}^L may be determined by line shape analysis [3]. In the early days of studying spin relaxation in liquids, spectra due to known patterns of hyperfine structure were simulated by varying ΔH_{pp}^L

until a match between the simulated and observed spectrum was obtained, e.g., [22]. Since 1993 [4], the previous accurate, but tedious process was replaced by rapid fitting techniques which are embodied in the program *Lowfit*. The interested reader may consult a comprehensive review of *Lowfit* together with an instructive example, in the Supplementary Information of ref [15]. Relevant to this work, *Lowfit* separates the ABS and DIS, finds χ from ABS, and computes ΔH_{pp}^{L} from the following:

$$\Delta H_{pp}^{L} = \Delta H_{pp}^{0}\left(-1+\sqrt{1+4\chi^2}\right)/2\chi^2 \tag{4}$$

where ΔH_{pp}^{0} is the peak-to-peak line width of the V. See Fig. 1 for a graphic depiction of DIS, ABS, and ΔH_{pp}^{0} of an experimental spectrum.

For homogeneously broadened lines for ^{14}N, HSE adds contributions to $\Delta H_{pp}^{L}(0)$ and $1/\gamma T_2^{eff}$ that are linear with C [23].

$$\Delta H_{pp}^{L}(0) = \lim_{C\to 0}\Delta H_{pp}^{L}(0) + \frac{2}{3}\left(\frac{2}{\sqrt{3}}\right)K_{ex}C/\gamma$$

$$1/T_2^{eff} = \lim_{C\to 0}\left(1/T_2^{eff}\right) + \frac{2}{3}K_{ex}C$$

For ^{14}N nitroxides, the well-known statistical factor 2/3 [23] takes into account that only 2/3 of the spin exchanges are observable. Thus,

$$K_{ex}C = \frac{3}{2}\left(\Delta 1/T_2^{eff}\right) = \frac{3}{2}\left(\frac{\sqrt{3}}{2}\gamma\Delta\Delta H_{pp}^{L}(0),\right) \tag{5}$$

where $\Delta 1/T_2^{eff} \equiv \left(1/T_2^{eff} - 1/\lim_{C\to 0} T_2^{eff}\right)$ and $\Delta\Delta H_{pp}^{L}(0) \equiv \left[\Delta H_{pp}^{L}(0) - \lim_{C\to 0}\Delta H_{pp}^{L}(0)\right]$.

For IHB lines, plots of $\Delta H_{pp}^{L}(0)$ vs. C are non-linear near the origin, curving downward as C decreases [14] because hyperfine coupling to protons (deuterons) produces more than 3 lines, therefore more spin exchange events are observable. This is demonstrated theoretically in Fig. 3 of ref. [14]. Let us refer to this non-linearity as the "curvature." For values of $K_{ex}C/\gamma > a_H$, where a_H (G) is an effective proton coupling constant, the additional lines coalesce yielding three homogenous lines of constant slope [14]. The curvature affects the value of the intercept to a linear fit to the data but affects the slope little. For example, a linear fit of Fig. 3 of ref. [14] yields K_{ex} that is within ± 5 % of the known (input) value; however, the intercept is larger than the input value. Let us call this the "intercept discrepancy" which is dependent on the number and distribution of the points fit. Thus, a plot of Eq. 5 where $\lim_{C\to 0} T_2^{eff}$ and $\lim_{C\to 0}\Delta H_{pp}^{L}(0)$ are replaced by the observed intercepts, are correct to an estimated ± 5 %.

3. Experimental

The nitroxide spin probe H-Tempol was purchased from Molecular Probes, Inc. and used as received. A 13.0-mM stock solution of H-Tempol was prepared in Millipore water and serially diluted to obtain solutions with C = 13.0 – 1.06 mM. Samples were drawn into open-ended polytetrafluoroethylene (PTFE - ID: AWG21) tubing obtained from Zeus. The tubing was

then folded in half, and the open ends were sealed with Seal-Ease plastic clay from Clay Adams, Inc. These samples were placed into a glass housing through which N_2 was passed for 8 hours to deoxygenate the samples. The sample to be studied was removed from the housing, quickly inserted into a quartz tube made by Wilmad Glass Co, with a hole in the bottom, and placed into the quartz dewar insert of a Bruker N_2 temperature controller residing in the microwave cavity (ER 4119HS, TE_{011}) of a Bruker EMXPlus EPR spectrometer. The microwave source was a 200-mW Gunn dual oscillator. In this arrangement, N_2 was used to control the sample temperature at 295 K and maintain the sample deoxygenated. CW EPR spectra were obtained with modulation amplitude, 0.1 G; modulation frequency, 100 kHz; time constant, 0.01 ms; sweep time, 2.5 s; field sweep, 50 G; and resolution, 10 mG. CWS were obtained with Bruker's Xenon software package at 20 power settings, fine tuning between each spectrum.

4. Results

Figure 1A shows a spectrum of 13.0 mM H-Tempol in deoxygenated toluene at 295 K at low microwave power (3.2 mW). The ABS and DIS components are presented in B and C, respectively. The residual, which is the difference in the observed spectrum and the sum of the ABS and DIS components, is displayed along the baseline of spectrum A, showing that a near-perfect fit is obtained showing only minor noise. The low-field, (lf) and high-field (hf) components of DIS are due to HSE plus a small DIS component due to a slight mismatch of the cavity which is evident in the center-field line (cf). Each of the ABS lines (B) was fit with a V line shape of peak-to-peak width ΔH_{pp}^{0} as indicated for the lf. From *Lowfit*, χ was determined and ΔH_{pp}^{L} was computed from Eq. 4.

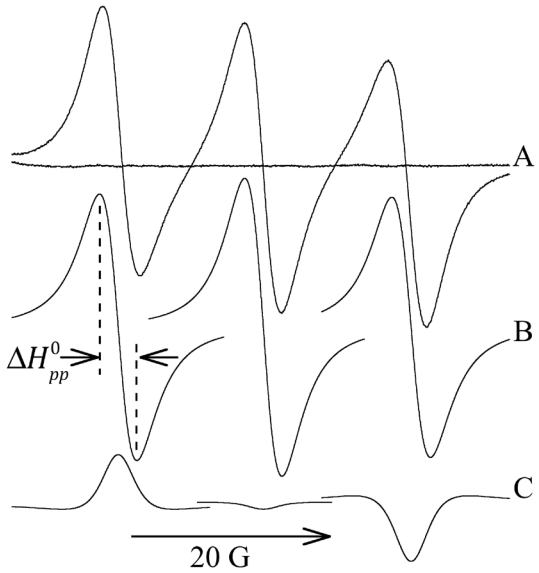

Fig. 1. (A) EPR spectrum of 13.0 mM H-Tempol in deoxygenated toluene at 295 K at low microwave power (3.2 mW). Decomposed ABS (B) and DIS (C) components. The peak-to-peak line width of the lf ABS is indicated. Observe that decomposition into ABS and DIS components is required to obtain both ΔH_{pp}^{0} and the shape of the ABS: there are no features on the spectrum itself that allow these parameters to be measured.

In Fig. 2A, the CWS of ΔH_{pp}^{L} for 1.06 mM H-Tempol, open symbols, and ΔH_{pp}^{0}, closed symbols are displayed showing that at small HSE, the deconvolution to obtain ΔH_{pp}^{L} is crucial, amounting to a factor of about two difference. Fig. 2B shows only the CWS of ΔH_{pp}^{L} for 13.0 mM H-Tempol. The corresponding values of ΔH_{pp}^{0} are larger but only about 10% and are not shown for clarity.

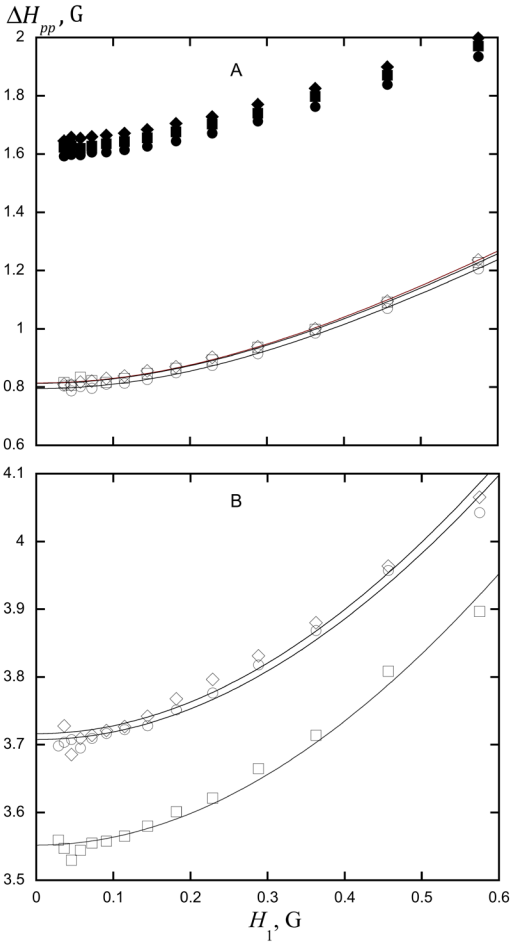

Fig. 2. (A) CWS of the Lorentzian line widths, ΔH_{pp}^{L}:C = 1.06 mM, open circles, lf, open squares, cf, open diamonds, hf; and the overall line widths, ΔH_{pp}^{0}: C = 1.06 mM, closed circles, lf, closed squares, cf, closed diamonds, hf. (B**)**. CWS of ΔH_{pp}^{L}: C = 13.0 mM, same symbols as in (A**)**. The CWS of ΔH_{pp}^{0} is not shown in (B**)**. Note that for 13.0 mM, ΔH_{pp}^{L} for cf is less than that for lf and hf as predicted by theory [24] while they are the same for 1.06 mM.

Fig. 3 shows the comparison between $K_{ex}C/\gamma$, Eq. 5, obtained from ESE and CW EPR. The ESE data were obtained from Fig. 3 of ref [13] utilizing WebPlot Digitizer (Copyright 2010 – 2020 Ankit Rohatgi). The EPR data were obtained by subtracting $\Delta H_{pp}^{L}(0)_{intercept}$= 0.65 ± 0.06 G. The ESE data were presented as $\Delta 1/T_2^{eff}$ with the intercept already subtracted in ref [13]. In spite of differences in the intercept discrepancy, Fig. 3 clearly shows that the slopes of the two methods are within experimental error of one another.

The fits of the data to Eq. 5 yield K_{ex}/γ = 310 ± 30 G/M for ESE and 305 ± 10 G/M CW EPR. The uncertainties are estimated from the fits.

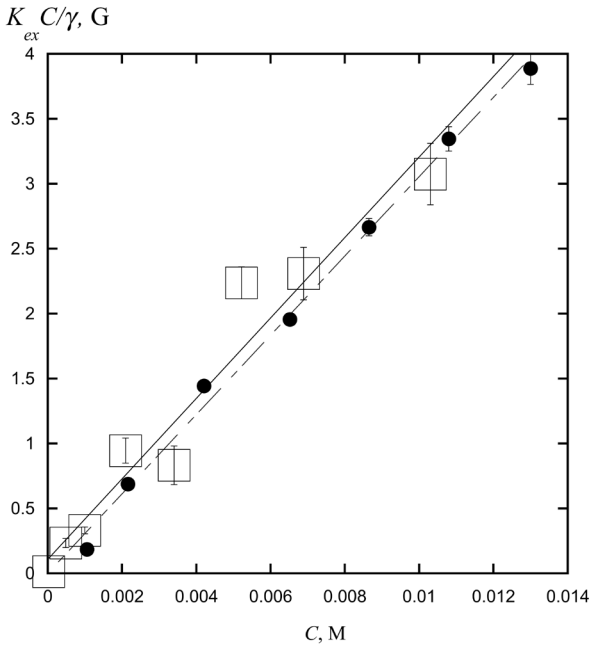

Fig. 3. Spin exchange frequency, $K_{ex}C/\gamma$, vs concentration for H-Tempol in toluene. open squares, ESE, room temperature [13]. Solid circles, CW EPR, 295 K, this work. Solid line, linear fit to ESE data, r = 0.973. Dashed line, linear fit to CW EPR data, r = 0.998.

5. Discussion and Conclusions

Fig. 3 shows that CW EPR and ESE report the same value of the spin exchange rate constant, K_{ex}, over a range of spin exchange frequencies accessible to both methods, affirming the main purpose of this Communication. For nitroxides with severe IHB such as H-Tempol solving the complications described here would be necessary if the true value of T_2^{eff} were desired.

For experiments designed to test theories, severely IHB nitroxides are not likely to be selected; rather, for example, Fremy's salt (a_H = 0) or perdeuterated 2,2,6,6-tetramethyl-4-oxopiperidine-1-oxyl (a_D = 0.010 – 0.018 G). For these nitroxides, the corrections to obtain the Lorentzian linewidth, ΔH_{pp}^L from Eq. 4, are still necessary (e.g., compare Figs. 11 a and b of ref. [14]); however, the curvature and the intercept discrepancy are less than 1 % so an accurate value of the true $\Delta H_{pp}^L(0)$ is found from the intercept of a linear fit.

We now turn to a brief discussion of the motivation to revive the CW EPR approach to study spin relaxation at large values of spin exchange frequencies. We have already mentioned that it would be interesting to study the relaxation of DIS [15] which is straightforward with CW EPR because it is separated from ABS. With present ESE methods, it is difficult to image how this could be accomplished. Fig. 2B shows that $\Delta H_{pp}^L(0)$ is different for cf relative to lf and hf, a difference that agrees quantitatively with theory [24]. It seems improbable that this difference could be uncovered by ESE both because of considerably lower precision but also because the lf and hf are superimposed with DIS while the cf is not. CW EPR is capable of studying $\Delta H_{pp}^L(0)$

to very large values (large values of $K_{ex}C/\gamma$) where the spectral lines merge and eventually narrow while values of T_2^{eff} accessible by ESE with present technology are limited. As the spin exchange frequency increases, another interesting fact predicted by theory and confirmed experimentally is the following: the doubly-integrated intensity of the lf and hf lines diminish while that of the cf increases such that the sum of the three remains proportional to C. In fact, theory predicts that above a critical value of $K_{ex}C/A_0$, where A_0 is the unsaturated ^{14}N hyperfine coupling constant, the intensity of lf and hf become zero and at higher value of spin exchange frequency become negative (emission). Finally, as already mentioned, recent theories [16-18] predict "peculiar" behaviors of all of the measurable parameters of both ABS and DIS. One such peculiar behavior has just been verified experimentally [19]. A summary of the other peculiar effects may be found in the SI of ref [19].

To summarize: the power of CW EPR derives from its ability to study the various manifestations of ABS and DIS separately under saturating conditions and extend these studies to large values of $K_{ex}C/\gamma$ inaccessible to pulse methods. The investigation of spin relaxation of ABS and DIS under conditions of HSE has just begun [15].

On a personal note, we have been approached at scientific meetings through recent years and posed the following question: why do you do such a complicated line-shape analysis when you could simply use ESE?" We are now ready with three answers: (1) the analysis is not complicated now that efficient line shape fitting methods are available, (2) we show here that the same results are obtained with CWS to significantly better precision, and (3) for large $K_{ex}C/\gamma$, current time responses of pulsed EPR spectrometers are not capable of measuring such short T_2-relaxation times.

Declaration of Competing Interest: None.

Acknowledgment

M.P. gratefully acknowledges support from NSF RUI (grant no. 1856746).

References

1. D. Marsh, *Spin-Label Electron Paramagnetic Resonance Spectroscopy*.(CRC Press. Taylor & Francis Group, Boca Raton, FL. USA, 2020)
2. A. Schweiger and G. Jeschke, *Principles of Pulse Electron Paramagnetic Resonance*.(Oxford University Press,, Oxford, UK; New York, 2001)
3. B.L. Bales, in *Biological Magnetic Resonance*, L.J. Berliner and J. Reuben, Editors. (Plenum, New York, 1989)
4. H.J. Halpern, M. Peric, C. Yu, and B.L. Bales, J. Magn. Reson. **103**, 13-22 (1993)
5. B.D. Armstrong and S. Han, J. Chem. Phys. **127**, 104508 (2007)
6. P.W. Percival and J.S. Hyde, J. Magn. Reson. **23**, 249-257 (1976)
7. C. Mailer, D.A. Haas, E.J. Husted, J.G. Gladden, and B.H. Robinson, J. Magn. Res. **91**, 475-496 (1991)
8. B.H. Robinson, D.A. Haas, and C. Mailer, Science **263**, 490-493 (1994)
9. B.H. Robinson, A.W. Reese, E. Gibbons, and C. Mailer, J. Phys. Chem. B. **103**, 5881-5894 (1999)

10. J.R. Biller, V. Meyer, H. Elajaili, G.M. Rosen, J.P.Y. Kao, S.S. Eaton, and G.R. Eaton, J. Magn. Reson. **212**, 370 - 377 (2011)
11. J.R. Biller, V.M. Meyer, H. Elajaili, G.M. Rosen, S.S. Eaton, and G.R. Eaton, J. Magn. Res. **225**, 52-57 (2012)
12. J.R. Biller, H. Elajaili, V. Meyer, G.M. Rosen, S.S. Eaton, and G.R. Eaton, J. Magn. Res. **236**, 47-56 (2013)
13. J.R. Biller, J.E. McPeak, S.S. Eaton, and G.R. Eaton, Appl. Magn. Reson. **49**, 1235 - 1251 (2018)
14. B.L. Bales, M.M. Bakirov, R.T. Galeev, I.A. Kirilyuk, A.I. Kokorin, and K.M. Salikhov, Appl. Magn. Reson. **48**, 1399-1445 (2017)
15. M.M. Bakirov, I.T. Khairuzhdinov, K.M. Salikhov, R.N. Schwartz, and B.L. Bales, Appl. Magn. Reson. **53**, 1275-1350 (2022)
16. K.M. Salikhov, Appl. Magn. Reson. **49**, 1417-1430 (2018)
17. K.M. Salikhov, Appl. Magn. Reson. **51**, 297-325 (2020)
18. K.M. Salikhov, Appl. Magn. Reson. **52**, 1063-1091 (2021)
19. B.L. Bales, M. Peric, I. Dragutan, M.K. Bowman, M.M. Bakirov, and R.N. Schwartz, J. Phys. Chem. Letters **13**, 10952-10957 (2022)
20. B.L. Bales and M. Peric, Appl. Magn. Reson. **48**, 175-200 (2017)
21. M.M. Bakirov, K.M. Salikhov, M. Peric , R.N. Schwartz, and B.L. Bales, Appl. Magn. Reson. **50**, 919-942 (2019)
22. W. Plachy and D. Kivelson, J. Chem. Phys. **47**, 3312-3318 (1967)
23. B.L. Bales and M. Peric, J. Phys. Chem. B **101**, 8707-8716 (1997)
24. B.L. Bales and M. Peric, J. Phys. Chem. A **106**, 4846-4854 (2002)

Graphical abstract